ISSN 1330-3651 (Print), ISSN 1848-6339 (Online)
Received: 27 March 2026; Accepted: 12 May 2026

https://doi.org/10.17559/TV-20260327003487
Original scientific paper

Research on Fracture Surface Search and Reconstruction Strategies for 3D Bone Fragment Stitching

Lei YIN, Weiwei CAO, Junqi LI, Weili SHI, Feng QU, Miao Yu, Zhengang JIANG*

Abstract: This study presents an automated three-dimensional (3D) fracture stitching framework for virtual fracture reduction, aiming to improve the accuracy and robustness of preoperative planning. Existing fracture registration methods often rely on Iterative Closest Point (ICP), which is sensitive to inaccurate initialization and prone to local convergence. Moreover, surface noise, fragment defects, and irregular fracture morphologies can cause unstable feature extraction and unreliable matching. To address these challenges, we propose a fracture-surface-aware coarse-to-fine registration framework rather than a direct combination of standard PCA, FPFH, and ICP modules. First, PCA-guided directional filtering and curvature-guided region growing are used to localize fracture-relevant surfaces, reducing interference from non-contact bone regions. Second, FPFH descriptors are embedded into a PCA-constrained coarse registration scheme, providing a more stable initialization than stochastic SAC-IA-based matching. Finally, a Full-Bidirectional ICP strategy is introduced, which retains mutual nearest-neighbor correspondences and minimizes a symmetric bidirectional error to suppress density-driven drift. Experiments on real and simulated fracture datasets demonstrate that the proposed method achieves improved registration accuracy, stability, and efficiency, indicating its potential for virtual fracture reduction and clinical surgical planning.

Keywords: bone fragment stitching; FPFH; fracture-surface extraction; full-bidirectional ICP; point cloud registration; virtual fracture reduction

1 INTRODUCTION

Automated fracture reduction is an emerging area of investigation within clinical fracture management. Despite significant advancements in three-dimensional (3D) model segmentation and registration techniques, the development of practical solutions for clinical fracture reduction remains limited. This limitation is primarily due to challenges posed by irregular fracture surfaces, heterogeneous fragment morphologies, and variable imaging quality.

Recent progress in virtual bone reduction has facilitated improvements in 3D reconstruction and surgical planning. Delgado et al. [1] provided a comprehensive review of virtual reduction technologies, delineating their fundamental components - namely, 3D visualization, model editing, and preoperative evaluation - and underscoring their clinical utility in decision-making processes. Building upon this foundation, Caiti, Zheng, and colleagues [2, 3] extended the application of 3D bone models to osteotomy planning and fragment positioning, thereby enhancing controllability and precision during preoperative design.

In the domain of geometric fragment matching, Buschbaum, Paulano and collaborators [4-8] introduced automated alignment methodologies leveraging curvature, normal vectors, and contact area metrics, demonstrating promising results on clean, standardized datasets. However, these approaches exhibit diminished performance when applied to clinical computed tomography (CT) data characterized by noise, thin fracture lines, and partial defects. Furthermore, their reliance on manual annotation of fracture lines or feature regions impedes full automation. Contra lateral mirroring techniques have been validated for bilaterally symmetric bones such as the calcaneus and femur [9-11]; nonetheless, their applicability is constrained in anatomically asymmetric structures like the pelvis and spine.

Collectively, existing methods depend heavily on surface integrity and frequently encounter issues of over- or under-extraction when processing authentic fracture data, thereby limiting their capacity to meet clinical demands for high-precision reduction. Consequently, the development of a fracture-surface extraction and matching framework tailored to real-world clinical scenarios is imperative for advancing automated surgical reduction systems.

To address these challenges, we proposed an enhanced PCA-guided three-dimensional region growing algorithm designed to achieve stable fracture-surface extraction in the presence of high-noise clinical data. Initially, PCA is employed to estimate the principal direction of the fracture, followed by PassThrough filtering to eliminate non-fracture points and mitigate seed interference. Subsequently, region growing is driven by normal vector consistency and local geometric constraints, facilitating robust extraction of irregular fracture surfaces. To improve initial alignment accuracy during registration, we integrate FPFH descriptors with PCA-based coarse registration and apply an improved ICPalgorithm for high-precision refinement. Experimental evaluations on both real and simulated fracture datasets demonstrate that the proposed method reliably extracts fracture surfaces despite noise, thin cortical disruptions, and structural defects, while substantially enhancing alignment accuracy and convergence speed.

Our main contributions are summarized as follows:

First, we propose a fracture-surface-aware extraction strategy that combines PCA-guided directional filtering with curvature-guided region growing. Unlike standard registration pipelines that compute descriptors on broadly sampled bone surfaces, the proposed strategy localizes fracture-relevant interfaces before registration. This reduces interference from non-contact cortical regions and improves the reliability of subsequent feature matching under noisy and incomplete clinical CT data.

Additionally, we develop a PCA-constrained FPFH coarse registration scheme. Instead of relying on purely stochastic SAC-IA sampling, the proposed method introduces PCA-derived principal directions as geometric orientation priors for fracture surfaces. FPFH descriptors are then used within this constrained search space to establish more stable correspondences, thereby improving

the robustness of initial pose estimation.

Furthermore, we introduce a Full-Bidirectional ICP refinement strategy for incomplete fracture interfaces. Different from conventional one-way ICP, the proposed method retains mutual nearest-neighbor correspondences through bidirectional KD-tree search and minimizes a symmetric bidirectional point-to-point error. This reduces density-driven bias and alleviates drift caused by missing surfaces, uneven point density, and limited overlap.

2 RELATED WORKS

2.1 Fracture-Surface Extraction

The extraction of fracture surfaces constitutes a critical preliminary step in virtual reduction and three-dimensional reconstruction processes, with its precision substantially influencing the effectiveness of subsequent registration and alignment procedures. Initial methodologies predominantly depended on manual delineation within two-dimensional slices or interactive segmentation of three-dimensional models. Although these techniques can yield highly accurate outcomes, they rely heavily on clinical expertise, are time-intensive, and susceptible to subjective variability. Advancements in geometric surface analysis have prompted researchers to explore automated identification of fracture regions by leveraging curvature and surface normal attributes. For instance, Buschbaum et al. [5] employed curvature and normal-shift features to detect femoral fracture lines, demonstrating promising results on well-preserved, low-noise bone models. Nevertheless, this approach exhibits sensitivity to noise and cortical defects when applied to actual CT data, resulting in misclassification errors. Similarly, Paulano et al. [6] introduced a curvature-based method for identifying contact regions to facilitate automatic reduction; however, this technique depends heavily on geometric completeness and exhibits instability in cases involving multiple fragments or extensively damaged surfaces. Vlachopoulos et al. [7] utilized curvature scale space to match proximal humerus fragments but required manual annotation of fracture cracks, thereby limiting the potential for full automation. In summary, geometry-driven extraction methods perform effectively on standardized and pristine models but are prone to over-segmentation, under-segmentation, or extraction of irrelevant features when confronted with artifacts, thin cortical fractures, uneven point density, or surface defects commonly present in clinical CT scans. To overcome these challenges, the present study proposes a PCA-guided fracture-surface extraction technique integrated with three-dimensional region growing, which substantially enhances robustness in handling irregular and clinically realistic fracture scenarios.

2.2 3D Point Cloud Coarse Registration

Coarse registration serves as the foundational step for fragment alignment by providing an initial pose estimate, and its precision critically influences the convergence and stability of subsequent fine registration processes. Conventional approaches often depend on PCA-based principal axis alignment or geometric centering to approximate the global transformation. However, due to the highly uneven distribution, presence of missing regions, and noise contamination commonly observed in fracture surfaces, reliance on PCA alone tends to result in instability. To enhance robustness, recent methodologies have incorporated local geometric descriptors to establish sparse feature correspondences, followed by global optimization of RANSAC, demonstrating favorable performance on complete bone surfaces or synthetic datasets. In the context of medical applications, Delgado et al. [1] emphasized the significance of virtual 3D reduction in preoperative planning, while Caiti [2] and Zheng et al. [3] employed three-dimensional models for osteotomy planning and fragment positioning, facilitating partial automation of coarse reduction. Another research avenue utilizes the contra lateral bone as a mirrored template, yielding notable outcomes for bilaterally symmetric anatomical structures such as the calcaneus and femur [9-11]. Nevertheless, this strategy is less applicable to anatomical regions lacking bilateral symmetry. To overcome the limitations of PCA-only alignment and descriptor-based matching in the presence of noisy and incomplete clinical point clouds, we propose a correspondence strategy that integrates FPFH descriptors with PCA-derived principal axes. This approach leverages the robustness of local feature descriptors for alignment while employing PCA to establish a stable reference coordinate frame, thereby enhancing the reliability of coarse registration under challenging conditions characterized by noise and data sparsity.

2.3 Fine Registration and Fracture Reduction

Fine registration seeks to attain high-precision alignment by refining an initial coarse pose, thereby facilitating the accurate repositioning of fracture fragments. A widely recognized method for this purpose is the ICP algorithm [12], which determines the optimal rigid transformation through iterative updates of point-to-point correspondences. To enhance computational efficiency and numerical stability, several improvements have been proposed, including KD-tree-accelerated nearest-neighbor searches [13], point-to-plane ICP, weighted ICP, and variants employing robust kernels. Nonetheless, in the context of authentic bone fracture models, valid correspondences are predominantly confined to the fracture surfaces, while extensive non-contact regions may lead to erroneous matches, causing the algorithm to converge to suboptimal local minima. To mitigate these challenges, hybrid registration strategies have been investigated. Such approaches integrate feature correspondences, bidirectional ICP, or local consistency constraints to enhance alignment accuracy. For example, Cheng et al. [22] combine SAC-IA feature matching with KD-ICP refinement, achieving improved precision through robust feature sampling and efficient local alignment. Despite these advancements, the intrinsic characteristics of clinical fracture data - such as irregularly missing fragments, noisy cortical boundaries, and limited overlapping areas - continue to pose significant challenges to the performance of standard ICP methods. Consequently, achieving robust fine registration in medical applications remains an open and active area of research.

Although the FPFH+SAC-IA+ICP pipeline has been

widely used for general point cloud registration, its direct application to clinical fracture reduction remains problematic. First, FPFH descriptors computed on broad or complete bone surfaces may include non-contact anatomical regions, which can introduce false correspondences that are irrelevant to fracture reduction. Second, SAC-IA depends on stochastic sampling of feature correspondences, making the initial pose estimation sensitive to noise, missing fragments, and limited overlap. Third, conventional ICP usually minimizes a one-way source-to-target distance and may therefore suffer from density-driven bias when the two fracture surfaces are incomplete or unevenly sampled. These limitations motivate the proposed fracture-surface-aware strategy, in which fracture interface localization, PCA-constrained FPFH coarse alignment, and symmetric Full-Bidirectional ICP refinement are coupled into a unified registration framework.

Recently, learning-based point cloud registration methods have attracted increasing attention. For example, Deep Closest Point (DCP) learns point cloud feature representations and estimates rigid transformations through a neural network-based matching framework, while GeoTransformer introduces geometric transformer representations for robust correspondence estimation under low-overlap conditions. These methods have demonstrated promising performance on general point cloud benchmarks. However, their direct application to clinical fracture-surface registration remains challenging because fracture surfaces are usually small, irregular, incomplete, and lack large-scale annotated paired training data. In addition, the generalization ability of networks trained on synthetic, indoor, or outdoor datasets to clinical fracture CT-derived point clouds is still uncertain. Therefore, in this study, learning-based methods are discussed as relevant recent developments, while the experimental comparison focuses on geometry-based registration methods that can be directly applied without task-specific training data.

3 METHOD

Fig. 1 illustrates the overall workflow of the proposed three-dimensional fracture-surface stitching framework. The pipeline consists of three coupled stages: fracture-surface extraction, coarse registration, and fine registration. The output of each stage is used as the input of the next stage, forming a coarse-to-fine registration process.

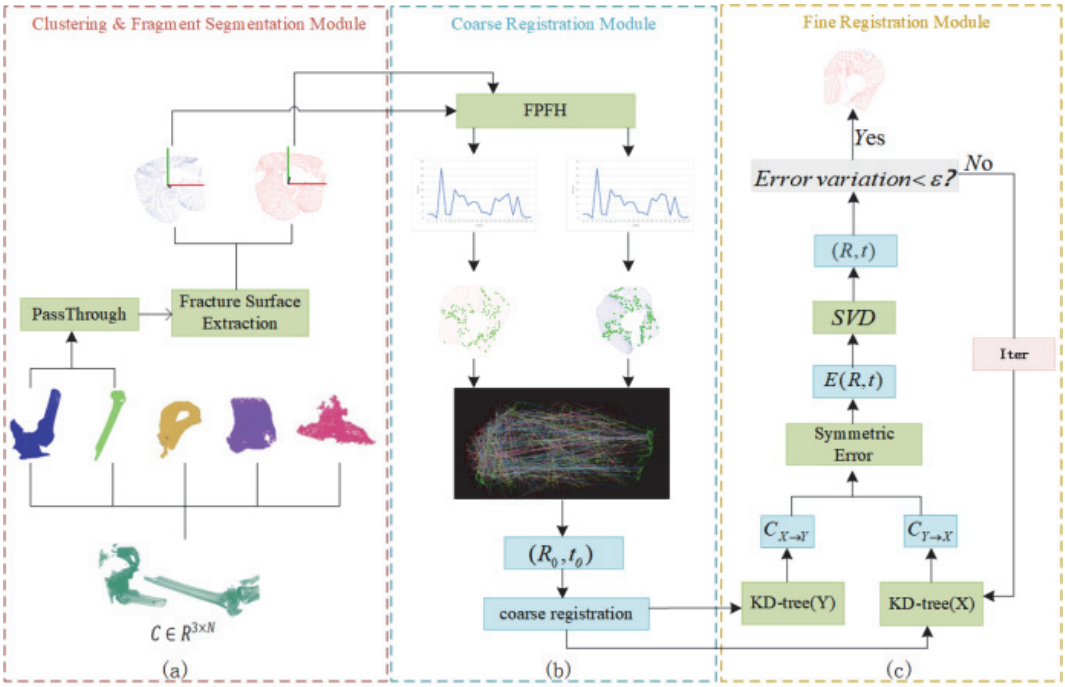

Figure 1 Overall workflow of the proposed fracture-surface-aware registration framework

First, the CT-reconstructed point cloud is segmented into individual bone fragments, and PCA-guided filtering followed by curvature-guided region growing is used to extract fracture-surface point clouds. Second, FPFH descriptors are computed on the extracted fracture surfaces, and PCA-derived orientation information is used to estimate an initial rigid transformation. Third, the coarsely aligned fracture surfaces are refined by Full-Bidirectional ICP, where mutual nearest-neighbor correspondences are constructed using bidirectional KD-trees and optimized with a symmetric point-to-point error. The final output is the registered bone fragment pair for virtual fracture reduction.

In the first stage, the CT-reconstructed point cloud is segmented into individual bone fragments by Euclidean clustering. For each fragment, PCA-guided directional filtering is performed along the principal axis to remove irrelevant non-fracture regions. Curvature-guided region growing is then applied to the filtered candidate region to obtain the fracture-surface point cloud.

In the second stage, the extracted fracture-surface point clouds are used for coarse registration. FPFH descriptors are computed only on these localized fracture surfaces rather than on the entire bone fragment surface. The FPFH correspondences provide local geometric matching information, while the PCA-derived principal directions provide a global orientation constraint. By combining these two types of information, an initial rigid

transformation $T_0 = (R_0, t_0)$ is estimated.

In the third stage, the initial transformation T_0 is used to roughly align the source fracture surface with the target fracture surface. Full-Bidirectional ICP is then performed to refine the alignment. KD-trees are constructed for both point clouds, and only mutual nearest-neighbor correspondences are retained. Finally, a symmetric bidirectional point-to-point error is minimized to obtain the refined transformation for virtual fracture reduction.

3.1 Fracture Surface Extraction via PCA-Guided Region Growing

The extraction of fracture surfaces is a fundamental step in virtual bone reduction, with its precision critically influencing both coarse and fine registration processes. Nonetheless, clinical point cloud data frequently present challenges such as irregular fracture morphologies, elevated noise levels, delicate thin-layer structures, and extraneous surface elements. These factors make traditional region-growing techniques unstable and susceptible to incomplete or inaccurate segmentation outcomes. To address these limitations and enhance extraction robustness, we propose a PCA-guided three-dimensional region-growing algorithm. Initially, the principal fracture direction is estimated via PCA, which imposes directional constraints to mitigate the expansion into irrelevant surface areas. Subsequently, a PassThrough filter is employed to preliminarily select candidate fracture regions, thereby narrowing the search space and augmenting computational efficiency. The region-growing procedure is then executed under constraints of normal vector consistency and local geometric features, facilitating the reliable extraction of complex and noisy fracture surfaces.

3.1.1 Point Cloud Generation and Preprocessing

The fractured bone is initially reconstructed into a three-dimensional STL mesh utilizing the Marching Cubes algorithm [14]. Subsequently, the STL mesh is transformed into a point cloud via voxel-based sampling, wherein the triangular mesh faces are systematically examined voxel-by-voxel, and points are generated atlocations where intersections between voxels and mesh surfaces occur. This method yields an initial point cloud that maintains the geometric intricacies of the fracture, providing a foundational basis for subsequent processes of surface extraction and registration.

$$C = \left\{ c_i \in R^3 \,\middle|\, i = 1, 2, \ldots, N \right\} \tag{1}$$

Each point in the cloud is denoted as:

$$c_i = (x_i, y_i, z_i) \in R^3 \tag{2}$$

Then, the point cloud was segmented by the Euclidean clustering method to obtain multiple cluster subsets $\{P_1, P_2, \ldots, P_M\}$, where each P_j represents an independent bone fragment.

3.1.2 Fracture Principal Axis Estimation Based on PCA

For each fracture fragment point cloud $P = \{p_i\}_{i=1}^m$ Principal Component Analysis estimates the principal axis of the fragment. The covariance matrix is defined as follows:

$$\begin{aligned} &M_{3\times3} = 1/m \sum_{i=1}^{m} (p_i - \overline{p})(p_i - \overline{p})^T, \\ &\overline{p} = 1/m \sum_{i=1}^{m} p_i \end{aligned} \tag{3}$$

Eigen-decomposition is performed on M:

$$\lambda V = MV \tag{4}$$

yielding eigenvalues and the corresponding eigenvectors:

$$\lambda_1 \le \lambda_2 \le \lambda_3, \quad V = (V_1, V_2, V_3) \tag{5}$$

where V_3 is associated with the largest eigenvalue, which represents the principal axis of the fracture fragment. Based on this, the point cloud is projected into the eigenvector space as follows:

$$project_i = (p_i - \overline{p}) \times V \tag{6}$$

3.1.3 PassThrough Filtering Based on Projected Coordinates

After estimating the principal axis of the point cloud, we define an interval $[T_{\min}, T_{\max}]$ along the axis to isolate the local region containing the fracture surface. The filtering interval was selected empirically according to the projected distribution of the point cloud along the PCA principal axis. To avoid sensitivity to bone size and point-cloud scale, we used a relative interval rather than a fixed absolute threshold. In our experiments, approximately 15% of the projection range near the potential fracture end was retained. This value was chosen based on empirical trials within 10%-25%, where smaller intervals tended to remove valid fracture-surface points, while larger intervals introduced excessive non-fracture cortical regions. Thus, the selected interval provides a balance between fracture-surface completeness and the exclusion of irrelevant surface points. The filtered point cloud is expressed as follows:

$$P' = \left\{ p_i \in P \,|\, T_{\min} < x_i < T_{\max} \right\} \tag{7}$$

This operation effectively removes many irrelevant points and significantly improves the computational efficiency of the subsequent region growing procedure.

3.1.4 Curvature-Guided Region Growing

To further extract the fracture surface from P', the surface normal and local curvature of each point is estimated, and an appropriate seed point is then selected to initialize the region-growing process. For a given point, its

k-nearest neighbors form the local covariance matrix:

$$S = \frac{1}{k}\sum_{i=1}^{k}(q_i - \bar{q})(q_i - \bar{q})^T \tag{8}$$

where $\bar{q}$ is the neighborhood centroid and q_i denotes the neighboring points. The surface normal is obtained by minimizing the following objective:

$$\min_n \sum_{i=1}^{k}\left(n^T \cdot (q_i - \bar{q})\right)^2 \tag{9}$$

Applying the Lagrange multiplier method leads to:

$$Sn = \lambda n, \quad \| n \|_2 = 1 \tag{10}$$

The eigenvector corresponding to the smallest eigenvalue λ represents the estimated normal direction. With eigenvalues ordered as $\lambda_1 \le \lambda_2 \le \lambda_3$, local curvature κ is computed as follows:

$$\kappa = \frac{\lambda_1}{\lambda_1 + \lambda_2 + \lambda_3} \tag{11}$$

A lower curvature value κ indicates that the local neighborhood is more planar and geometrically stable. The point exhibiting the minimal curvature is chosen as the initial seed. For each potential neighboring point, assessments are conducted based on both the deviation in normal angle and the difference in curvature; points meeting the predefined thresholds for these criteria are incorporated into the region. This procedure is iteratively repeated until no additional points qualify for inclusion.

3.2 FPFH-Enhanced PCA-Based Fracture Surface Registration

The input to this stage is the pair of fracture-surface point clouds extracted in Section 3.1. The output is an initial rigid transformation $T_0 = (R_0, t_0)$, which provides the initialization for the subsequent Full-Bidirectional ICP refinement.

Following fracture-surface extraction, a stable initial alignment is required before fine registration. In standard FPFH+SAC-IA pipelines, the initial transformation is estimated by stochastic sampling of feature correspondences. However, for clinical fracture surfaces, the overlap is often limited and the descriptors may be affected by noise, missing boundaries, and irregular geometries. This may cause SAC-IA to select geometrically inconsistent correspondences and produce unstable initial poses.

To address this issue, we introduce a PCA-constrained FPFH coarse registration strategy. The extracted fracture surfaces are first analyzed by PCA to obtain their principal directions, which provide a global orientation prior for the relative alignment. FPFH descriptors are then computed on the localized fracture interfaces rather than on the entire bone fragment surface. By combining local FPFH descriptors with PCA-derived orientation constraints, the proposed coarse registration reduces the search ambiguity and improves the robustness of initial transformation estimation.

3.2.1 Local Coordinate Construction and Feature Computation

For a query point p_q and one of its neighboring points p_k, a local reference frame is first constructed using the normal vector of p_q:

$$u = n_q, v = \frac{(p_k - p_q)\times u}{\left\|(p_k - p_q)\times u\right\|_2}, w = u \times v \tag{12}$$

where n_q denotes the surface normal at p_q. Based on this coordinate system, three angular geometric features are computed:

$$\begin{aligned} \alpha &= v^T n_k, \\ \phi &= u^T \frac{p_k - p_q}{\left\|p_k - p_q\right\|_2}, \\ \theta &= a\tan 2\left(w^T n_k, u^T n_k\right) \end{aligned} \tag{13}$$

Together, these three quantities describe the local geometric configuration between the query point and its neighbors.

3.2.2 SPFH and FPFH Feature Construction

For each point, a histogram of the above local geometric features is generated, forming the simplified FPFH descriptor SPFH:

$$\mathrm{SPFH}(p_q) = Hist\left(\{\alpha_i, \phi_i, \theta_i\}_{i=1}^{k}\right) \tag{14}$$

To enhance the stability of the descriptor, weighted accumulation of neighborhood features is introduced, producing the final FPFH descriptor:

$$\begin{aligned} &\mathrm{FPFH}(p_q) = \mathrm{SPFH}(p_q) + \\ &\frac{1}{k}\sum_{i=1}^{k} w_i \,\mathrm{SPFH}(p_{q,i}), \quad w_i = \frac{1}{\left\|p_q - p_{q,i}\right\|_2} \end{aligned} \tag{15}$$

where $p_{q,i}$ denotes the i-th neighboring point of p_q, and w_i is the distance-based weight. The cumulative approach enhances robustness against noise, incomplete surface data, and irregular fracture geometries. Utilizing the computed FPFH feature vectors, correspondence pairs between two fracture surfaces are identified within the feature space. Subsequently, PCA is employed to determine the principal orientation of each surface, thereby establishing an initial rotational constraint. Finally, the rotation matrix and translation vector are derived from the matched feature pairs, achieving the preliminary alignment.

This coarse registration phase furnishes a dependable initial pose for subsequent fine registration, thereby improving convergence stability and computational efficiency.

3.3 Full-Bidirectional ICP

The initial transformation obtained from the PCA-constrained FPFH coarse registration is used to initialize the fine registration stage. After applying this transformation, the source and target fracture surfaces are approximately aligned, allowing the subsequent ICP refinement to focus on local geometric adjustment rather than global pose search.

Following the extraction of fracture surfaces and initial coarse registration, achieving a higher degree of registration accuracy is essential for the precise reconstruction of bone fragments. While the conventional ICP algorithm is relatively straightforward, it often experiences drift in scenarios where the fracture surface is incomplete, contaminated with noise, or exhibits uneven point density. Consequently, this limits its effectiveness for high-precision medical reconstruction tasks. To overcome these challenges, we introduce a Full-Bidirectional ICP algorithm designed to improve robustness and stability during the fine registration process.

3.3.1 Bidirectional KD-Tree Correspondence Search

Let the coarsely aligned point clouds be designated as the source set X and the target set Y. To guarantee robust correspondence determination, a bidirectional KD-tree nearest-neighbor approach is utilized:

$$K_X = \mathrm{KDTree}(Y), \quad K_Y = \mathrm{KDTree}(X) \tag{16}$$

Nearest-neighbor queries are performed in both directions. To guarantee matching consistency, only mutual nearest-neighbor pairs are retained:

$$\tilde{C} = \left\{(x,y) \middle| (x,y) \in \tilde{C}_{X\to Y} \text{ and } \tilde{C}_{Y\to X}\right\} \tag{17}$$

Bidirectional matching helps eliminate incorrect correspondences caused by missing surfaces or noise, improving stability for subsequent optimization.

3.3.2 Symmetric-Error Model

The ICP algorithm exclusively minimizes the unidirectional point-to-point distance from the source to the target, a limitation that frequently results in drift when applied to incomplete fracture interfaces. To address this issue, we proposed a symmetric-error model that concurrently minimizes the bidirectional alignment error.

$$E(R,t) = \sum_{(x,y)\in\tilde{C}} \left\| Rx + t - y \right\|_2^2 + \sum_{(x,y)\in\tilde{C}} \left\| x - R^T(y-t) \right\|_2^2 \tag{18}$$

where $R \in SO(3)$ is the rotation matrix and $t \in \mathbb{R}^3$ is the translation vector. The first term aligns X toward Y, while the second term maps Y back to X. This dual constraint avoids density-driven bias and yields more stable alignment for incomplete fracture surfaces.

3.3.3 Transformation Estimation and Iteration

Given correspondence set $\tilde{C}$, the symmetric-error can be linearized and solved for R and t using SVD.

Center the correspondence pairs:

$$\tilde{x} = x - \bar{x}, \quad \tilde{y} = y - \bar{y} \tag{19}$$

where $\bar{x}$ and $\bar{y}$ denote the centroids of the corresponding source and target points, respectively. Construct covariance matrix:

$$H = \sum_{(x,y)\in\tilde{C}} \tilde{x}\tilde{y}^T \tag{20}$$

Perform SVD:

$$H = U\Sigma V^T \tag{21}$$

Compute rotation and translation:

$$R = VDU^T, \quad D = diag\left(1,1,\det(VU^T)\right) \tag{22}$$

$$t = \bar{y} - R\bar{x} \tag{23}$$

The transformation (R, t) is subsequently applied to update the source point cloud, and the processes of correspondence search and optimization are iteratively performed until convergence is achieved.

4 EXPERIMENTS

The experimental data utilized in this study were obtained from the orthopedics dataset provided by Jilin University Medical College. Three-dimensional reconstruction of CT images was carried out using Visual Studio 2022 in conjunction with the Visualization Toolkit (VTK). Procedures including point cloud segmentation, fracture surface extraction, and registration were executed employing the Point Cloud Library (PCL). All experiments were performed on a computing system configured with an Intel Core i7-10700 process or operating at 2.9 GHz and equipped with 8 GB of RAM.

4.1 Experimental Setup

The experimental dataset consisted of two groups: real clinical fracture models and simulated fracture models. The real-data group included three CT-derived fracture models, denoted as Real Fracture I, Real Fracture II, and Real Fracture III. These models were reconstructed from clinical CT data and contained irregular fracture surfaces, noise, missing regions, and incomplete boundaries. The simulated-data group included five virtual fracture models, denoted as Simulated Fracture I-V. Compared with the real

fracture models, the simulated models generally had smoother fracture surfaces and more regular geometric structures. Therefore, the dataset contains eight experimental samples in total, including three real clinical fracture models and five simulated fracture models. The real fracture models were mainly used to evaluate robustness under clinically realistic conditions, while the simulated models were used to evaluate registration performance under more controlled geometric conditions.

To improve reproducibility, the main parameter settings used in the experiments are further specified. In the PCA-guided filtering stage, the retained interval was set to approximately 15% of the PCA projection range near the potential fracture end, as described in Section 3.1.3. For curvature-guided region growing, surface normals and local curvatures were estimated using the k-nearest neighbors of each point, with $k = 30$. The smoothness threshold and curvature threshold were set to 3° and 1.0, respectively. For FPFH-based coarse registration, the normal estimation radius and FPFH descriptor radius were set according to the average point spacing of the fracture-surface point cloud. Specifically, the normal estimation radius was set to approximately three times the average point spacing, and the FPFH descriptor radius was set to approximately five times the average point spacing. For Full-Bidirectional ICP refinement, the maximum number of iterations was set to 100, and the convergence threshold was set to 10^{-6}. Bidirectional nearest-neighbor matching was performed using KD-tree search, and only mutual nearest-neighbor pairs were retained for symmetric-error optimization. The same parameter settings were used for all real and simulated fracture models unless otherwise specified.

4.1.1 Evaluation Metrics

Mean Squared Error (MSE) [15]: MSE quantifies the average squared Euclidean distance between the transformed source points and their corresponding target points. A lower MSE value indicates higher registration accuracy. The metric is formally defined as follows:

$$\mathrm{MSE} = \frac{1}{N}\sum_{i=1}^{N}\left\|Rx_i + t - y_i\right\|_2^2 \tag{24}$$

Hausdorff Distance (HD) [16]: The Hausdorff Distance servesas a metric for quantifying the geometric dissimilarity between two sets of points. It is defined as the greatest distance from any point in one set to the closest point in the other set. Formally, the definition is provided as follows.

$$d_H(X', Y) = \max\left\{\begin{array}{l}\sup\limits_{x'\in X'}\inf\limits_{y\in Y}\left\|x' - y\right\|_2, \\ \sup\limits_{y\in Y}\inf\limits_{x'\in X'}\left\|y - x'\right\|_2\end{array}\right\} \tag{25}$$

Root Mean Square Error (RMSE) [17]: RMSE is a widely utilized metric for assessing reconstruction accuracy. RMSE measures the root mean square Euclidean distance between the transformed source points and their corresponding target points, and is formally defined as follows.

$$\mathrm{RMSE} = \sqrt{\frac{1}{N}\sum_{i=1}^{N}\left\|Rx_i + t - y_i\right\|_2^2} \tag{26}$$

4.1.2 Competing Methods

In recent years, substantial advancements have been made in point cloud registration, particularly in the areas of global search, local optimization, and geometric representation. Schirmer et al. [18] introduced Semantic NDT, a method that integrates semantic constraints into the Normal Distributions Transform framework. This integration facilitates rapid and robust global initialization, thereby providing a dependable initial pose for subsequent refinement processes. Zhou et al. [19] developed a technique for constructing stable feature correspondences by employing ISS key points alongside 3D Shape Context descriptors. This approach significantly enhances the reliability of global registration and establishes a robust correspondence foundation for subsequent local refinement. Regarding local fine registration, Singandhupe et al. [20] proposed ESM-ICP, which improves the optimization performance of the ICP algorithm by formulating a novel similarity matrix through exponential mapping. This innovation leads to faster convergence rates and increased robustness in the presence of noisy point clouds. Lv et al. [21] embedded the ICP algorithm within the Kendall shape space framework and applied shape normalization to mitigate the effects of scale and rotational variations, thereby enhancing local registration robustness in scenarios involving complex deformations. Additionally, Cheng et al. [22] combined the Sample Consensus Initial Alignment (SAC-IA) method for global transformation estimation with a KD-tree - accelerated ICP for local refinement. This hybrid registration pipeline, termed SAC-IA + KD-ICP, achieves high alignment accuracy even when confronted with substantial pose discrepancies.

4.2 Performance

4.2.1 Fracture Surface Extraction Experiments

To assess the efficacy of the proposed fracture surface extraction technique, several long-bone fracture models reconstructed from clinical CT scans were selected as test specimens. The original bone surfaces exhibited common imaging-related imperfections, including noise, voids, and partial discontinuities, which can substantially hinder fracture-interface detection and subsequent registration processes. Consequently, each dataset was subjected to a sequential workflow comprising preprocessing, fracture-plane localization, and fracture surface extraction. The resulting extracted interfaces were subsequently visualized and quantitatively analyzed to evaluate the method's applicability and robustness across diverse fracture geometries.

A comparative analysis between the conventional region growing algorithm and the enhanced region growing method developed herein revealed that the traditional approach is inadequate for effectively extracting fracture surface points from authentic clinical datasets.

Specifically, in simulated fracture models, the conventional algorithm frequently generated numerous scattered point clusters, necessitating additional manual intervention to accurately identify the true fracture plane.

Conversely, as illustrated in Fig. 2, the improved region-growing algorithm introduced in this study enables the direct extraction of the fracture-surface point cloud. During preprocessing, irrelevant point clusters are eliminated while preserving regions pertinent to the fracture plane, thereby ensuring that the subsequent region growing process concentrates on the structural surface of interest. This refinement enables the proposed method to demonstrate greater robustness when applied to real fractured bone data, yielding more precise and consistent interface extraction.

In conclusion, the comparative experiments unequivocally indicate that the traditional region growing algorithm exhibits significant limitations, whereas the enhanced version attains superior performance in fracture-section extraction, characterized by increased accuracy and automation.

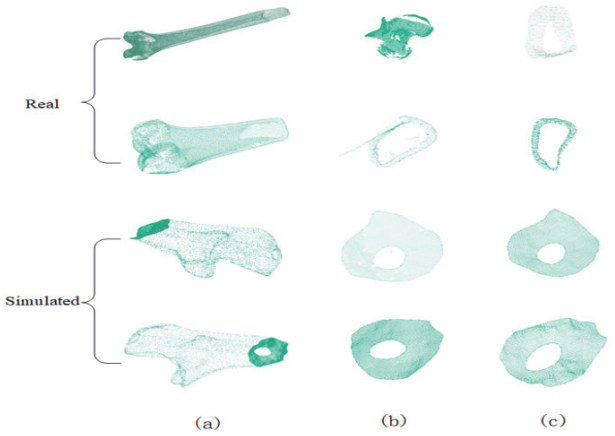

Figure 2 (a) Original fractured bone point cloud; (b) fracture surface extracted using the conventional region growing algorithm; (c) fracture surface extracted using the proposed method. It can be observed that, compared with the region-growing result where boundary discontinuities and irregular noise remain, the proposed method produces a more complete, smoother and better-defined fracture surface even under complex fracture conditions. The extracted interface shows significantly improved continuity and robustness

4.2.2 Quantitative Analysis

To evaluate the registration performance under different data conditions, the quantitative results are reported separately for real clinical fracture models and simulated fracture models. The real fracture models contain irregular fracture surfaces, incomplete boundaries, noise, and CT reconstruction artifacts, and are therefore used to evaluate robustness under clinically realistic conditions. In contrast, the simulated fracture models generally have smoother fracture surfaces and more regular geometries, and are used to evaluate the registration performance under more controlled conditions.

In Tabs. 1-4, "-" indicates that the corresponding method did not produce a valid registration result under the same experimental settings. Failure cases include incorrect alignment, local convergence, insufficient reliable correspondences, or non-meaningful transformations. Therefore, RMSE or runtime was not reported for these cases.

Table 1 RMSE comparison on real fracture models

Method	Real I	Real II	Real III
NDT+ICP	-	-	-
3DCS+ICP	-	-	-
4PCS+ICP	-	-	-
PCA	-	-	-
PCA+ICP	-	-	-
SAC-IA+ICP	0.472986	0.653193	-
Ours	0.433252	0.575827	0.850666

Results on real fracture models. Tab. 1 reports the RMSE results on the three real fracture models. It can be observed that most conventional registration methods fail to obtain valid results on real clinical fracture data. This is mainly because the reliable overlapping region is limited to the fracture surface, while non-fracture cortical regions, noise, and incomplete boundaries can introduce unstable correspondences.

The comparison with SAC-IA+ICP is particularly important because it represents a standard FPFH-based coarse-to-fine registration pipeline. Compared with SAC-IA+ICP, the proposed method achieves lower RMSE on Real Fracture I and Real Fracture II, where both methods produce valid registration results. Moreover, the proposed method obtains a valid result on Real Fracture III, whereas SAC-IA+ICP fails in this case. This improvement can be attributed to two methodological differences. First, the proposed method performs FPFH matching on extracted fracture surfaces rather than on broad bone surfaces, reducing the influence of non-contact regions. Second, the PCA-derived principal directions provide an orientation prior for coarse alignment, reducing the dependence on stochastic correspondence sampling in SAC-IA. These results indicate that the proposed fracture-surface-aware coarse-to-fine strategy improves registration robustness when fracture surfaces are noisy, incomplete, or have limited overlap.

Results on simulated fracture models. Compared with real clinical fracture data, the simulated fracture models generally have smoother fracture surfaces, fewer reconstruction artifacts, and more regular geometric structures. Therefore, more registration methods can achieve valid coarse registration on simulated models, as shown in Tab. 2. However, their stability and accuracy still vary across different cases. The proposed method maintains stable registration performance on the simulated fracture models, indicating that it can also handle controlled fracture geometries effectively.

Table 2 RMSE comparison on simulated fracture models $\times 10^{-4}$

Method	Sim I	Sim II	Sim III	Sim IV	Sim V
NDT+ICP	-	36.88	-	-	-
3DCS+ICP	-	61.66	1.843	1.169	1.108
4PCS+ICP	-	54.67	1.467	9.134	-
PCA	-	26.26	7.219	2.669	33.13
PCA+ICP	-	0.898	0.072	1.832	0.642
SAC-IA+ICP	453.1	0.885	35.29	3.719	0.642
Ours	433.2	0.884	0.072	0.534	0.642

The results on simulated fracture models further show the difference between real clinical data and controlled virtual models. Compared with real fracture cases, the simulated models generally contain smoother fracture

surfaces, fewer reconstruction artifacts, and more regular geometric structures. Therefore, more registration methods can obtain valid results on simulated models. However, their performance remains inconsistent across cases. Methods such as 3DCS+ICP and 4PCS+ICP can be efficient in some cases, but their registration accuracy is less stable. PCA+ICP and SAC-IA+ICP can provide reasonable alignment when the fracture geometry is smooth, but they are more sensitive to initialization and may require higher computational cost. In contrast, the proposed method maintains stable registration performance by combining fracture-surface localization, PCA-constrained FPFH coarse registration, and Full-Bidirectional ICP refinement.

Runtime on real fracture models. Tab. 3 reports the registration time on the three real fracture models. Since most conventional methods fail to produce valid registration results on real clinical fracture data, their runtime is not reported. Among the valid cases, SAC-IA+ICP requires substantially longer processing time than the proposed method. This is mainly because SAC-IA depends on stochastic feature correspondence sampling, which increases the computational burden when the fracture surfaces are noisy, incomplete, or have limited overlap. By contrast, the proposed method reduces the search space through PCA-guided fracture-surface extraction and uses PCA-derived orientation constraints to improve coarse initialization. As a result, it achieves shorter runtime while maintaining lower RMSE on the valid real fracture cases.

Table 3 Runtime comparison on real fracture models.

Method	Real I	Real II	Real III
NDT+ICP	-	-	-
3DCS+ICP	-	-	-
4PCS+ICP	-	-	-
PCA	-	-	-
PCA+ICP	-	-	-
SAC-IA+ICP	52.50 s	144.0 s	-
Ours	33.78 s	26.83 s	27.43 s

The runtime results on real fracture models further support the efficiency of the proposed strategy. Compared with SAC-IA+ICP, the proposed method reduces the computational cost by narrowing the registration region to the extracted fracture surfaces and by using PCA-derived orientation constraints for coarse alignment. In addition, Full-Bidirectional ICP improves refinement stability by retaining mutual nearest-neighbor correspondences. These results indicate that the efficiency gain comes from the coupled design of fracture-surface localization, PCA-constrained FPFH coarse registration, and bidirectional refinement.

Runtime on simulated fracture models. Tab. 4 reports the registration time on simulated fracture models. Compared with real fracture data, more baseline methods can be executed on simulated models because the fracture surfaces are smoother and the geometric structures are more regular. However, the runtime varies considerably among different methods. PCA+ICP and SAC-IA+ICP often require longer computational time, whereas 3DCS+ICP and 4PCS+ICP can be faster in some cases but may sacrifice registration accuracy. The proposed method achieves a favorable balance between accuracy and efficiency across the simulated fracture models.

Table 4 Runtime comparison on simulated fracture models

Method	Sim I	Sim II	Sim III	Sim IV	Sim V
NDT+ICP	-	12.76 s	-	-	-
3DCS+ICP	-	26.32 s	17.74 s	0.413 s	25.60 s
4PCS+ICP	-	0.41 s	0.715 s	1.182 s	-
PCA	-	1.22 s	4.777 s	21.68 s	1.017 s
PCA+ICP	-	80.04 s	132.0 s	48.15 s	71.89 s
SAC-IA+ICP	144.2 s	167.5 s	2.516 s	12.67 s	144.2 s
Ours	33.78 s	2.955 s	26.69 s	0.574 s	33.78 s

Additional Hausdorff Distance evaluation. In addition to RMSE, Hausdorff Distance (HD) was further reported to provide a more comprehensive evaluation of the final reduction accuracy. RMSE reflects the average registration error, whereas HD measures the maximum geometric discrepancy between two point sets and is more sensitive to local boundary mismatch and worst-case surface deviation. For real fracture cases, the reduced fracture model was compared with the mirrored contralateral bone model. For simulated fracture cases, the reduced model was compared with the corresponding complete reference model. The additional HD results are summarized in Tab. 5.

Table 5 Hausdorff Distance of final reduction results

Data	HD / mm
Sim I	0.135
Sim II	0.120
Sim III	0.104
Sim IV	0.132
Sim V	0.112
Real I	25.36
Real II	37.82
Real III	51.59

The HD results provide complementary evidence to the RMSE-based evaluation. For real fracture cases, the HD values are larger because the reduced fragments are compared with mirrored contralateral bone models, where anatomical asymmetry, CT reconstruction artifacts, incomplete fracture boundaries, and limited overlap may increase the maximum surface discrepancy. In contrast, the simulated fracture models have complete reference models and smoother fracture geometries, resulting in much smaller HD values. Therefore, the real and simulated datasets evaluate different aspects of the proposed method: real fracture data assess robustness under clinically realistic conditions, whereas simulated models assess final reduction accuracy under controlled geometric conditions.

Comparison with Existing Approaches and Clinical Implications. Compared with conventional PCA-based registration, the proposed method is less dependent on global principal-axis estimation alone. PCA-only methods may become unstable when fracture surfaces are incomplete, noisy, or geometrically irregular, whereas the proposed framework restricts registration to fracture-relevant surfaces and further uses FPFH descriptors to establish local geometric correspondences. Compared with standard FPFH+SAC-IA+ICP pipelines, the proposed method avoids performing descriptor matching on broad bone surfaces and reduces the dependence on stochastic correspondence sampling by introducing PCA-derived orientation constraints. Compared with conventional one-way ICP, Full-Bidirectional ICP improves correspondence reliability by retaining mutual nearest-neighbor pairs and minimizing a symmetric bidirectional error, which helps reduce density-driven drift under incomplete overlap.

Nevertheless, the proposed method still has several limitations. Its performance may degrade when the fracture surface is extremely incomplete, when the overlap between fragments is very limited, or when CT-derived point clouds contain severe noise and reconstruction artifacts. Under these conditions, PCA-based direction estimation, FPFH correspondence construction, and bidirectional ICP refinement may all become less stable. In addition, the current framework is primarily based on geometric features and does not incorporate anatomical priors or learning-based shape constraints, which may limit its performance in highly comminuted or complex multi-fragment fractures.

From a clinical perspective, the proposed method provides a training-free and interpretable framework for virtual fracture reduction. By automatically extracting fracture surfaces and improving registration stability, it has the potential to reduce manual intervention in preoperative planning and provide surgeons with more reliable fragment alignment references. This may contribute to improved surgical planning efficiency and more accurate virtual reduction, especially for clinical cases where fracture boundaries are irregular or incomplete.

4.2.3 Qualitative Analysis

This section presents qualitative experiments performed on both authentic clinical fracture models reconstructed from CT scans and synthetic fracture samples. The objective is to assess the visual registration accuracy and robustness of the proposed method across diverse bone structures and varying data conditions. By comparing the reconstruction and surface alignment performance of multiple algorithms, we demonstrate the method's capability to manage irregular geometries, missing fragments, and noise interference. The results indicate that the proposed approach consistently achieves smooth and precise fracture alignment in both real and simulated datasets, thereby providing a reliable basis for subsequent quantitative evaluations.

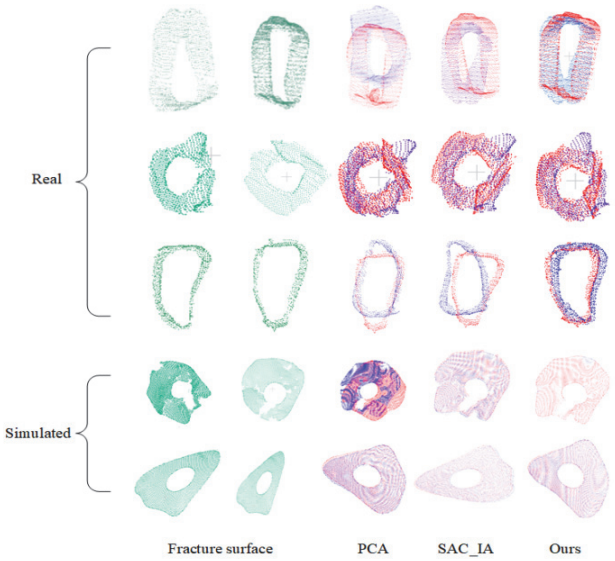

Figure 3 Comparison of coarse registration results of fracture surfaces on real and simulated bone datasets. From left to right: extracted fracture surfaces, PCA-based coarse registration results, SAC_IA-based coarse registration results, and the results of our proposed method. The first three rows correspond to fracture surfaces of real bones, and the last two rows correspond to fracture surfaces of simulated fracture models. Compared with traditional registration methods, the proposed method exhibits higher registration accuracy and smoother surface matching

The comparative analysis presented in Fig. 3 reveals substantial variation in the performance of different methods for coarse registration of fracture surface point clouds. Given the inherent complexity and irregularity of actual fracture surfaces, PCA-based registration methods are prone to becoming trapped in local optima, which leads to suboptimal alignment accuracy. Although the SAC_IA approach can provide an approximate initial alignment, its effectiveness is constrained by surface defects and geometric irregularities. In contrast, the coarse registration algorithm introduced in this study exhibits enhanced robustness in fracture surface localization, feature extraction, and initial pose estimation, thereby delivering the most reliable coarse registration in the majority of cases. It is also observed that when the fracture surface is relatively smooth, all three methods yield comparable performance in coarse registration.

By integrating the proposed coarse registration technique with the bidirectional KD-tree accelerated Full-Bidirectional ICP algorithm, a comprehensive virtual reduction of fractured bone fragments is accomplished. The final reduction outcome is illustrated in Fig. 4.

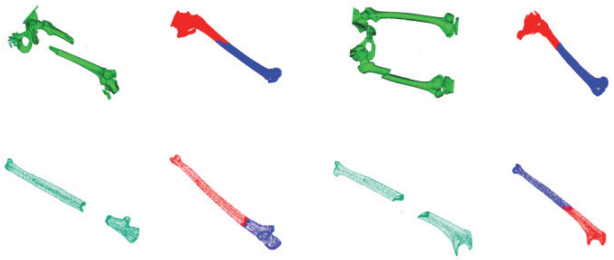

Figure 4 The reduction results of the real fracture and the simulated fracture model. The top image shows the reduction result of the real fracture model, and the bottom image shows the reduction result of the simulated fracture model. This method can achieve accurate and stable fracture reconstruction, and good reduction performance is obtained in both types of data

As illustrated by the real and simulated fracture reduction outcomes presented in Fig. 4, the integration of the enhanced coarse registration technique with the bidirectional KD-tree - augmented Full-Bidirectional ICP algorithm exhibits distinct advantages in virtual fracture reduction. This approach facilitates highly precise alignment for both authentic and simulated fracture models, thereby ensuring superior registration accuracy and establishing a robust basis for medical analysis and surgical planning. Furthermore, the method demonstrates consistent stability across diverse conditions, including complex geometrical configurations, noisy or incomplete real fracture surfaces, as well as simulated datasets, indicating strong robustness. Additionally, the incorporation of the bidirectional KD-tree substantially accelerates nearest-neighbor searches, decreasing computational time without sacrificing accuracy, which in turn enhances the efficiency of clinical workflows.

5 SUMMARY

Fracture reconstruction and the alignment of bone fragments continue to be pivotal areas of investigation within orthopedic medical computing. To overcome the difficulties associated with fracture surface detection and the reassembly of three-dimensional bone fragments, this study introduces a novel approach to extracting and registering point clouds of fracture-surface point clouds.

Initially, CT data are reconstructed into three-dimensional geometries and subsequently transformed into point clouds. Euclidean clustering is then employed to isolate individual fracture fragments. The principal axes of each point cloud are determined through PCA, followed by the application of PassThrough filtering to localize the fracture region. An enhanced region-growing algorithm is subsequently utilized to facilitate precise extraction of the fracture surfaces. For the reconstruction phase, the segmented fracture surfaces undergo alignment via an improved PCA-based coarse registration technique, which is further refined through a Full-Bidirectional ICP refinement based on bidirectional KD-tree correspondence search for fine matching. Experimental evaluations demonstrate that the proposed methodology achieves accurate and robust identification of fracture surfaces and effective alignment of fragments, indicating significant potential for applications in virtual fracture reduction and preoperative surgical planning.

Despite the improved performance, the proposed method still has several limitations. The method may become less stable when the fracture surface is extremely incomplete, when the overlap between fragments is very limited, or when CT-derived point clouds contain severe noise and reconstruction artifacts. These conditions may affect PCA-based principal direction estimation, FPFH correspondence construction, and Full-Bidirectional ICP refinement. Future work will focus on adaptive parameter selection, stronger noise suppression, and hybrid registration strategies incorporating anatomical priors.

Acknowledgments

The project is supported by the first batch of Innovative Research Team at Zhongshan Institute of Changchun University of Science and Technology (No. CXTD2023010).

6 REFERENCES

[1] Jiménez-Delgado, J. J., Paulano-Godino, F., Pulido-Ramírez, R. et al. (2016). Computer assisted preoperative planning of bone fracture reduction: simulation techniques and new trends. *Medical Image Analysis*, *30*, 30-45. https://doi.org/10.1016/j.media.2015.12.005

[2] Caiti, G., Dobbe, J. G. G., Strackee, S. D. et al. (2019). Computer-assisted techniques in corrective distal radius osteotomy procedures. *IEEE Reviews in Biomedical Engineering*, *13*, 233-247. https://doi.org/10.1109/rbme.2019.2928424

[3] Zheng, Y., Chen, J., Yang, S. et al. (2022). Application of computerized virtual preoperative planning procedures in comminuted posterior wall acetabular fractures surgery. *Journal of Orthopaedic Surgery and Research*, *17*(1), 51. https://doi.org/10.1186/s13018-022-02937-5

[4] Lu, S. et al. (2023). Preoperative virtual reduction planning algorithm of fractured pelvis based on adaptive templates. *IEEE Transactions on Biomedical Engineering*, *70*(10), 2943-2954. https://doi.org/10.1109/tbme.2023.3272007

[5] Buschbaum, J., Fremd, R., Pohlemann, T. et al. (2015). Computer-assisted fracture reduction: A new approach for repositioning femoral fractures and planning reduction paths. *International Journal of Computer Assisted Radiology and Surgery*, *10*, 149-159. https://doi.org/10.1007/s11548-014-1011-2

[6] Paulano-Godino, F. & Jiménez-Delgado, J. J. (2017). Identification of fracture zones and its application in automatic bone fracture reduction. *Computer Methods and Programs in Biomedicine*, *141*, 93-104. https://doi.org/10.1016/j.cmpb.2016.12.014

[7] Vlachopoulos, L., Székely, G., Gerber, C. et al. (2018). A scale-space curvature matching algorithm for the reconstruction of complex proximal humeral fractures. *Medical Image Analysis*, *43*, 142-156. https://doi.org/10.1016/j.cmpb.2016.12.014

[8] Liu, B., Zhang, S., Zhang, J. et al. (2019). A personalized preoperative modeling system for internal fixation plates in long bone fracture surgery - A straightforward way from CT images to plate model. *The International Journal of Medical Robotics and Computer Assisted Surgery*, *15*(5), e2029. https://doi.org/10.1002/rcs.2029

[9] Wan, L., Yin, Q. S., Zhang, Y. et al. (2008). Computer-aided design of complicated calcaneal fracture by virtual mirror image. *Journal of Clinical Rehabilitative Tissue Engineering Research*, *12*(48), 9443-9446. https://doi.org/10.3969/j.issn.1673-8225.2008.48.015

[10] Song, Q., Li, T., Xia, H. et al. (2023). Three-dimensional printed cast assisted screw fixation of calcaneal fractures: A prospective study. *BMC Musculoskeletal Disorders*, *24*, 802. https://doi.org/10.1186/s12891-023-06927-4

[11] Zhang, W., Liu, J., Wang, X. M., & Li, D. S. (2018). The application of fracture recovery techniques based on 3D printing and three-dimensional data correction scheme in fractures of the proximal femur. Semantic Scholar. *Corpus ID: 228671870.*

[12] Besl, P. J. & McKay, N. D. (1992). Method for registration of 3-D shapes. *Sensor Fusion IV: Control Paradigms and Data Structures*, *1611*, 586-606. https://doi.org/10.1117/12.57955

[13] Rusinkiewicz, S. & Levoy, M. (2001). Efficient variants of the ICP algorithm. *Proceedings Third International Conference on 3-D Digital Imaging and Modeling*, 145-152. https://doi.org/10.1109/im.2001.924375

[14] Jolliffe, I. (2011). Principal component analysis. *International Encyclopedia of Statistical Science*, 1094-1096. https://doi.org/10.1007/978-3-642-04898-2_455

[15] Lorensen, W. E. & Cline, H. E. (1987). Marching cubes: A high resolution 3D surface construction algorithm. *ACM SIGGRAPH Computer Graphics*, *21*(4), 163-169. https://doi.org/10.1145/37401.37422

[16] Hou, Y. (2022). Global mean square error separation loss. *Journal of Physics: Conference Series*, *2363*(1), 012007. https://doi.org/10.1088/1742-6596/2363/1/012007

[17] Shekhar, S. & Xiong, H. (2008). Root-Mean-Square Error. *Encyclopedia of Gis*, 979-979. https://doi.org/10.1007/978-0-387-35973-1_1142

[18] Schirmer, R., Vaskevicius, N., Biber, P. et al. (2024). Fast global point cloud registration using semantic NDT. *2024 IEEE/RSJ International Conference on Intelligent Robots and Systems (IROS)*, 8831-8838. https://doi.org/10.1109/iros58592.2024.10801863

[19] Zhou, Z. X., Huang, D. D., & Liu, Z. (2023). Point cloud registration algorithm based on 3D shape context features (ISS+3DSC). *Journal of Applied Optics*, *44*(2). https://doi.org/10.5768/jao202344.0202005

[20] Singandhupe, A., Lokhande, S., & La, H. M. (2025). Registration of 3D Point Sets Using Exponential-based Similarity Matrix. https://arxiv.org/abs/2505.04540

[21] Lv, C., Lin, W., & Zhao, B. (2022). KSS-ICP: Point Cloud Registration Based on Kendall Shape Space. *IEEE Transactions on Image Processing*, *32*, 1681-1693. https://doi.org/10.1109/tip.2023.3251021

[22] Cheng, Y., Chu, H., Li, Y. et al. (2024). A hybrid improved SAC-IA with a KD-ICP algorithm for local point cloud alignment optimization. *Photonics*, *11*(7), 635. https://doi.org/10.3390/photonics11070635

Contact information:

Lei YIN
College of Computer Science and Technoloy,
Changchun University of Science and Technology,
Changchun, Jilin, 130021, China

Weiwei CAO
College of Computer Science and Technoloy,
Changchun University of Science and Technology,
Changchun, Jilin, 130021, China

Junqi LI
College of Computer Science and Technoloy,
Changchun University of Science and Technology,
Changchun, Jilin, 130021, China

Weili SHI
College of Computer Science and Technoloy,
Changchun University of Science and Technology,
Changchun, Jilin, 130021, China

Feng QU
College of Computer Science and Technoloy,
Changchun University of Science and Technology,
Changchun, Jilin, 130021, China
Zhongshan Institute of Changchun University of Science and Technology

Miao YU
College of Computer Science and Technoloy,
Changchun University of Science and Technology,
Changchun, Jilin, 130021, China

Zhengang JIANG
(Corresponding author)
College of Computer Science and Technoloy,
Changchun University of Science and Technology,
Changchun, Jilin, 130021, China
E-mail: jiangzhengangcust@163.com